IEEE Access
Multidisciplinary ⋮ Rapid Review ⋮ Open Access Journal

Received 3 January 2024, accepted 7 January 2024, date of publication 11 January 2024, date of current version 22 January 2024.

Digital Object Identifier 10.1109/ACCESS.2024.3353047

RESEARCH ARTICLE

Research on Encounter Probability Between a Supercavitating Vehicle and a Target Based on Path Planning

YANG GUANG, LU FAXING, XU JUNFEI, WU LING, AND LI YIYUAN
College of Weapon Engineering, Naval University of Engineering, Wuhan 430000, China

Corresponding author: Lu Faxing (lufaxing1974@163.com)

This work was supported in part by the National Natural Science Foundation of China under Grant 11774432.

ABSTRACT Supercavitating vehicles have received significant attention in military applications due to their high underwater speed. This paper aims to establish analytic models of the encounter probability between a supercavitating vehicle and its target in two modes: straight-running mode (SRM) and turning-straight-running mode (TSRM). Mathematical models for the supercavitating vehicle to encounter the target in SRM and TSRM are proposed. An improved particle swarm optimization (PSO) algorithm based on local best topology with a penalty function is introduced to plan the TSRM path of the supercavitating vehicle. The particle swarm position is updated by using Cauchy and Gaussian distributions. The judgement indexes of the encounter probability analytic models in SRM and TSRM are determined through statistical analysis. Based on the law of error propagation, the analytic models of judgement index variances in the two modes are derived by using the implicit function differential method, and the integral intervals of their probability density functions are obtained according to the relative motion between the supercavitating vehicle and the target. Monte Carlo simulations and hypothesis testing are utilized to verify the accuracy and feasibility of the encounter probability analytic models in SRM and TSRM.

INDEX TERMS Supercavitating vehicle, encounter probability, path planning, Monte Carlo method, law of error propagation.

I. INTRODUCTION

Supercavitating vehicles adopt supercavitation technology to achieve drag reduction and speed enhancement, and their underwater speed can reach more than 200kn. Owing to its high speed, it possesses substantial kinetic energy, excellent penetration capabilities, cost-effectiveness, and no casualties on our side, which makes it a potential means for underwater and surface target attacks with broad military application prospects [1]. Given the significant differences in hydrodynamic performance between supercavitating vehicles and conventional underwater vehicles, both domestic and foreign scholars have employed experimental and numerical simulation methods to investigate the hydrodynamic performance [2], [3], [4] and cavitation morphology [5], [6], [7] of supercavitating vehicles in recent years. Additionally, the presence of supercavity results in a sharp reduction in the buoyancy of the vehicle, thus leading to longitudinal motion instability. Consequently, numerous scholars have conducted studies on the longitudinal motion control of supercavitating vehicles based on the standard model proposed in the paper [8]. By considering the cavitation memory effect, changes of fan submerged depth over time [9], and other measures, the dynamic model of the supercavitating vehicle has been continuously refined, and control methods including H_∞ control [10], sliding mode control [11], neural network control [12], predictive control [13] have been proposed to effectively maintain its longitudinal motion stability. Due to the large noise generated by the cavitation collapse [14] and the structural limitation of supercavitating vehicles, the installation of guidance devices presents a significant challenge. Consequently, SRM remains the primary

The associate editor coordinating the review of this manuscript and approving it for publication was Diego Oliva.

attack mode for supercavitating vehicles. However, the initial heading of the supercavitating vehicle may not align with the straight-running mode with an advanced angle. Solely relying on the SRM could result in missed strike opportunities and low encounter probabilities. Therefore, it is necessary to study the turning-straight-running mode to enhance the operational flexibility and diversity of supercavitating vehicles. Currently, there is relatively little research on the TSRM of supercavitating vehicles. Besides their lateral maneuvering ability is the key factor to TSRM. Compared to other studies on supercavitating vehicles, there is a scarcity of research focused on their lateral maneuvering capabilities. In literature [15], numerical simulation methods were established to analyze and study the cavitation shape and forces during the rotation process of the supercavitating vehicle. In literature [16], the μ-synthesis control method was used to control the pitch channel and the yaw-roll channel separately to achieve Bank-to-turn of a supercavitating vehicle. Literature [17] proposed estimation methods for the minimum turning radius of a supercavitating vehicle and the maximum deflection angle of cavitation. Motivated by the previous research on the lateral rotation of supercavitating vehicles, the adaptive sliding mode control method based on neural networks is proposed to assess the lateral maneuvering ability of a supercavitating vehicle on the premise that the actuators did not fail [18].

Based on previous research on supercavitating vehicles both domestically and internationally, the research focus has been mainly on motion control, while relatively limited attention given to its military applications. In this paper, the encounter probability between the supercavitating vehicle and the target is studied. The encounter probability serves as a pivotal metric to evaluate the effectiveness of weapon systems and make decisions about weapon operation. The basis for calculating encounter probability lies in establishing an encounter model. Literatures [19], [20], and [21] established torpedo firing models and hitting conditions under various attack modes according to geometric relationships. Due to the limitation of the lateral maneuvering ability of the supercavitating vehicle, the turning-straight-running path cannot solely rely on the geometric relationship, but also needs to be planned according to the target motion parameters, situation information, and maneuvering ability of the supercavitating vehicle. Both domestic and foreign scholars have conducted extensive research on the path planning of unmanned vehicles. The primary methods include classical methods (such as Dubins curve [22], artificial potential field method [23]), heuristic algorithms (including A$*$ algorithm [24], particle swarm optimization algorithm [25], ant colony algorithm [26]), as well as deep reinforcement learning [27].

The current methods for calculating encounter probabilities primarily consist of the statistical method and analytic approaches. The statistical method based on the Monte Carlo method is widely used to calculate hit probability. Literature [28] applied the Monte Carlo method to analyze the statistical characteristics of hit probability in a rectangular target area. The literatures [29] and [30] evaluated the combat effectiveness of the anti-torpedo combat system and the surface ship torpedo defense system based on the Monte Carlo method. In literatures [31], [32], and [33], the Monte Carlo method was used to simulate the discovery, capture, and penetration probability of various torpedoes, respectively. Although the Monte Carlo method has the advantages of a simple concept and easy implementation, its calculation accuracy heavily depends on the number of simulations, which is unsuitable for real-time calculations, but more suitable for theoretical research [34] rather than actual combat applications. In contrast, the analytic method can directly calculate the encounter probability by establishing a mathematical model. Literatures [35] and [36] derived the coordinates of the torpedo at the target trajectory and the distance deviation, respectively, considering the errors based on the geometric relationship. The analytic solutions for the hit probability were then calculated by taking the target length and half-length as integral intervals without accounting for the influence of the target scale. Moreover, the two papers directly incorporated the mean square error of variables into the analytic model, which does not satisfy the statistical characteristics of probability. In literature [37], an analytic model for the target detection probability of a straight-running torpedo was established by using the error transmission theorem, considering only one-dimensional target position dispersion. Literature [38] treated the one-time turning-angle strike of the supercavitating torpedo as equivalent to the straight-running strike and built an analytic model for the hit probability by using the implicit function differential method. However, the encounter model is limited as it is solely based on geometric relations without considering the initial course, the maneuvering ability as well as rotational angular velocity error. Literature [34] takes the electromagnetic launched anti-torpedo torpedo as the research object. The mean square deviation of the heading angle is obtained by the implicit function differential method, and the capture probability is obtained by integration.

The purpose of this paper is to establish analytic models of the encounter probability between a supercavitating vehicle and a target in two modes: SRM and TSRM. Firstly, encounter models in two modes are established. The SRM utilizes the advanced angle mode, while the TSRM employs an improved particle swarm optimization algorithm for path planning. Subsequently, based on the Monte Carlo statistical analysis method, the statistical characteristics of the encounter probability considering the target scale are analyzed, and the judgement indexes of the encounter probability in two modes are determined by using the X-axis coordinate of the intersection point between the supercavitating vehicle path and the target path in the target coordinate system and miss distance, respectively. The interval estimation and hypothesis testing are employed to further validate that

the judgement indexes obey the standard normal distribution. Finally, the analytic calculation strategies of encounter probabilities in two modes are proposed. Considering the random error of each variable comprehensively, the mean square errors of the judgement indexes are derived by the implicit function differential method based on the law of error propagation [39]. The integral intervals of analytic models are determined according to the relative motion between the supercavitating vehicle and the target. The accuracy of the encounter probability analytic model proposed in this paper is validated compared with Monte Carlo simulation results.

II. ENCOUNTER MATHEMATICAL MODEL

The supercavitating vehicle model adopted in this paper is illustrated in Fig. 1, which is widely adopted in the study of motion control [12], [40], [41]. The encounter models between the supercavitating vehicle and the target in two modes are derived, and the encounter situation is depicted in Fig. 2. $X_EO_EZ_E$ and $X_BO_BZ_B$ represent the geodetic horizontal coordinate system and target coordinate system, respectively. The origin of $X_EO_EZ_E$ is located at the initial position of the supercavitating vehicle, with O_EX_E pointing northward. The origin of $X_BO_BZ_B$ is placed at the equivalent rectangular center of the target, with O_BX_B indicating the navigation direction. To facilitate subsequent analysis and formula derivation, several reasonable assumptions are made.

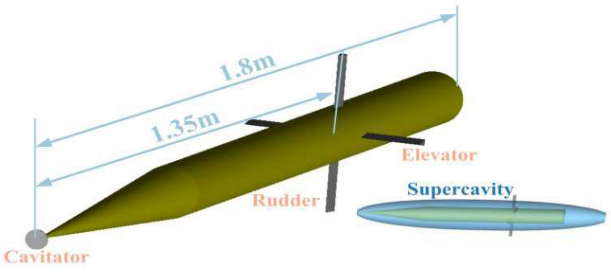

FIGURE 1. Supercavitating vehicle.

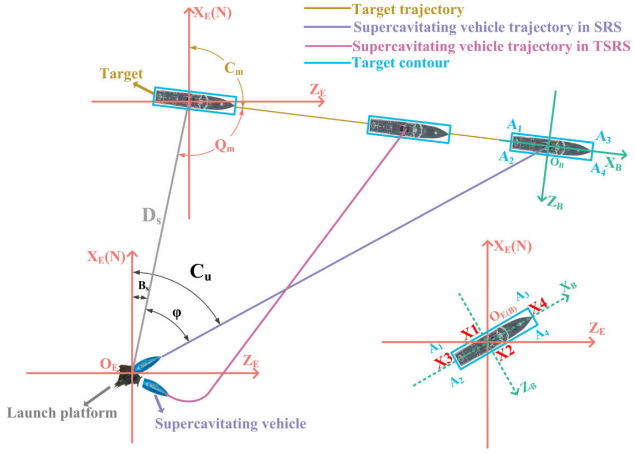

FIGURE 2. Encounter situation diagram and reference frames.

1. Given the speed of the supercavitating vehicle surpasses that of the target, the target is assumed to move uniformly in a straight line during the approach of the supercavitating vehicle.

2. The horizontal projection of the target ship in the geodetic coordinate system is approximately a rectangle with length L_m and width B_m.

3. In comparison to the target size, the supercavitating vehicle is equivalent to a point.

A. STRAIGHT-RUNNING MODE

The SRM of the supercavitating vehicle adopts the advanced angle mode. Sensor detection information includes azimuth B_s, range D_s, target heading C_m, and target speed V_m. The bearing angle can be expressed as follows.

$$Q_m = B_s - C_m - \pi\, sign(B_s - C_m) \tag{1}$$

where $Q_m \in [-\pi, \pi]$, Q_m is specified to be positive on the starboard side of the target.

According to the encounter triangle, the initial heading of the supercavitating vehicle in SRM should satisfy as follows.

$$C_u = B_s + \varphi \tag{2}$$

where the advanced angle can be expressed as $\varphi = ac\sin(V_m \sin Q_m / V_s)$. V_s represents the speed of the supercavitating vehicle. It can be seen that the advanced angle is only related to the velocity ratio between the target and the supercavitating vehicle.

Then the trajectory of the supercavitating vehicle in SRM can be expressed as follows.

$$\begin{cases} x^E_{s\_s} = V_s t_s \cos(C_u) \\ z^E_{s\_s} = V_s t_s \sin(C_u) \end{cases} \tag{3}$$

B. STRAIGHT-RUNNING MODE

From the encounter model in SRM, the heading of the supercavitating vehicle needs to satisfy the initial heading in SRM, which is easy to lose the opportunity to strike. To address the problem that the actual initial heading C_{ut} of the supercavitating vehicle does not meet the requirement of SRM, the supercavitating vehicle can employ turning-straight-running mode. The rotational angular velocity w of the supercavitating vehicle, turing-running time t_t and straight-running time t_s are the decision variables that need to be determined. w is specified to be positive when the supercavitating vehicle turns clockwise. In $X_EO_EZ_E$, the path of the supercavitating vehicle in TSRM and the target can be expressed as (4) and (5), respectively. Additionally, the total range of the supercavitating vehicle cannot exceed its limit range and the turning angle should not exceed one complete circle. There exist multiple path planning schemes to guide the supercavitating vehicle to the target centroid, which is not conducive to decision-making obviously. To enhance the optimization strategy while ensuring the encounter with the target centroid, the minimum navigation time constraint of the supercavitating vehicle is introduced, effectively screening out unfavorable

decision schemes. In summary, the objective function of the encounter between the supercavitating vehicle and the target centroid can be expressed as (6).

$$\begin{cases} x^E_{s\_ts} = \dfrac{V_s}{w}\sin(C_{ut}+wt_t) - \dfrac{V_s}{w}\sin(C_{ut}) \\ +V_s t_{ts}\cos(C_{ut}+wt_t) \\ z^E_{s\_ts} = -\dfrac{V_s}{w}\cos(C_{ut}+wt_t) + \dfrac{V_s}{w}\cos(C_{ut}) \\ +V_s t_{ts}\sin(C_{ut}+wt_t) \end{cases} \tag{4}$$

$$\begin{cases} x^E_m = D_s\cos(B_s) + V_m(t_t+t_{ts})\cos(C_m) \\ z^E_m = D_s\sin(B_s) + V_m(t_t+t_{ts})\sin(C_m) \end{cases} \tag{5}$$

$$\begin{cases} \min f = t_t + t_s \\ s.t. \begin{cases} d = \sqrt{(x^E_{s\_ts}-x^E_m)^2 + (z^E_{s\_ts}-z^E_m)^2} \le 10^{-6} \\ w \in [-40^\circ/_s, 40^\circ/_s] \\ t_t \in (0, {}^{2\pi}/_w) \\ t_{ts} \in (0, (L_{\max} - V_s t_t)/V_s] \end{cases} \end{cases} \tag{6}$$

According to the objective function, this problem is an optimization problem with multiple decision variables and constraints. PSO is a typical heuristic optimization algorithm renowned for its fast convergence and strong adaptability [42]. Nevertheless, it is prone to premature convergence, which leads to local optimal decision variables. This problem arises from the classical PSO algorithm's utilization of a global search approach within the solution space. As a result, when the particle swarm is updated in the vicinity of the local optimal, it is difficult to escape from the local optimal solution. To address this problem, a local best (lbest) topology is used for information exchange among particles [43], [44], as depicted in Fig. 3. The lbest topology empowers particles to search for optimal solutions within their neighborhood topology and achieves enhanced global search capability by moderating the convergence speed. Particle position update employs Cauchy and Gaussian distributions instead of particle velocity, as detailed in (7). The strategy of particle position update serves to increase population diversity and further prevent particle swarm from falling into local optimum [42]. For the encounter distance constraint d, a penalty function is introduced into the optimization algorithm, and a penalty factor is introduced into the fitness value of particles that do not meet the constraint, as shown in (8). The pseudocode of the Cauchy-Gaussian-penalty-PSO (CG-P-PSO) for the path planning of supercavitating vehicles is presented in the Fig. 4.

$$P_j^{i+1} = \begin{cases} lbest_j^i + \mathcal{N}(0,1)\left|pbest_j^i - lbest_j^i\right|, & rand > 0.5 \\ pbest_j^i + \mathcal{C}(1)\left|pbest_j^i - lbest_j^i\right|, & otherwise \end{cases} \tag{7}$$

$$f(P_j^i) = \begin{cases} f(P_j^i), & if\ d(P_j^i) - 10^{-6} \le 0 \\ f(P_j^i) + \lambda\left|d(P_j^i) - 10^{-6}\right|, & otherwise \end{cases} \tag{8}$$

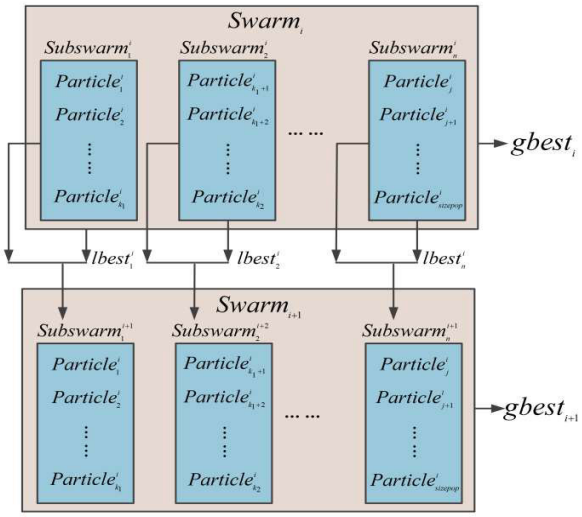

FIGURE 3. Local best topology.

Algorithm: improved PSO with constraints based on Cauchy and Gaussian distributions

Create and initialize $Swarm_1$ with particles P_j^1, $j \in [1, popsize]$, each with 3 dimensions;
Evaluate the objective function $f(P_j^1) \rightarrow gbestfitness^1$ and $pbestfitness_j^1$
Obtain $gbest^1$ and $pbest_j^1$
Construct local best topology $Subswarm_n^1$, $n \in [1, sizetopology] \rightarrow lbest_n^1$
for i=2:maxiteration
  for each particle $j \in [1, popsize]$ in $Swarm_{i-1}$ **do**
    for particles $P_{j\,in\,n}^{i-1}$ in $Subswarm_n^{i-1}$
      Update particle position according to Eq.(6)$\rightarrow P_{j\,in\,n}^i \rightarrow f(P_{j\,in\,n}^i)$
    end
    if $d(P_{j\,in\,n}^i) - 10^{-6} > 0$ **then**
      Add penalty value to $f(P_{j\,in\,n}^i)$ according to Eq.(7)
    end
    if $pbestfitness_j^{i-1} < f(P_{j\,in\,n}^i)$ **then**
      $pbestfitness_j^i = pbestfitness_j^{i-1}$
    else
      $pbestfitness_j^i = f(P_{j\,in\,n}^i)$
    end
  end
  Update $lbest_n^i$ in each $Subswarm_n^i$
  Obtain $gbestfitness^i$
  if $gbestfitness^{i-1} < gbestfitness^i$ **then**
    $gbestfitness^i = gbestfitness^{i-1}$
  end
end termination criterion is met;

FIGURE 4. Pseudocode of CG-P-PSO.

where P_j^{i+1} represents the jth particle in the $(i+1)th$ particle swarm. $\mathcal{C}(1)$ and $\mathcal{N}(0,1)$ denote parameters following Cauchy and Gaussian distributions, respectively. $pBest_j^i$ represents the optimal particle position. $lbest_{\mathrm{n}}^i$ represents the best particle position in the nth local neighborhood. $rand$ is a random number with a uniform distribution between 0 and 1. λ denotes the penalty factor.

To verify the stability and accuracy of the CG-P-PSO algorithm proposed in this paper, the Monte Carlo method is employed to plan the path of the supercavitating vehicle. The relevant parameters are detailed in Table 1, and penalty factor

TABLE 1. Operational situation information.

Target						Supercavitating vehicle	
D_s(m)	C_{M}(°)	B_s(°)	Q_m(°)	V_m(kn)	C_u(°)	C_{ut}(°)	V_s(kn)
6000	90	45	135	30	53.1301	83.1301	150

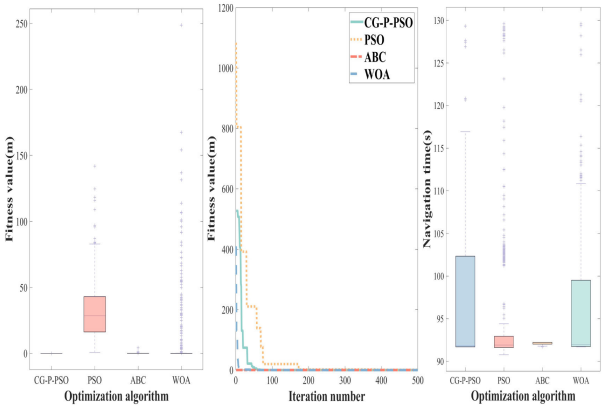

FIGURE 5. Comparison of results by optimization algorithm.

is $\lambda = 10^{-20}$. The Monte Carlo simulation is conducted 500 times. In each Monte Carlo simulation experiment, the particle swarm evolves 500 times, and the population size is 80. The simulation results are compared with those obtained from the classical PSO, artificial bee colony (ABC), whale optimization algorithm (WOA), as shown in Fig. 5. The inertial factor of classical PSO adopts the method in literature [45]. It can be seen from the box plot of encounter distance fitness values that CG-P-PSO algorithm exhibits the best performance in terms of accuracy and stability. Accordingly, the search process of four optimization algorithms with the minimum fitness value of encounter distance in 500 Monte Carlo experiments is plotted. The convergence rate of the CG-P-PSO is slower than that of ABC and WOA due to the lbest topology structure, but it can converge within 100 iterations in general, which meets the practical requirements. The box plot of shortest navigation time obtained from four optimization algorithms is presented in Table 2. The shortest navigation time across all Monte Carlo simulations is from classical PSO. However, the corresponding encounter distance fitness value is 63.0513m, which evidently does not meet the encounter requirements. Among the other three optimization algorithms, the shortest navigation time is obtained from both CG-P-PSO and WOA. Owing to the introduction of the penalty mechanism to CG-P-PSO, the shortest navigation time occurs 75 times among the 500 Monte Carlo simulations, while it only occurs once in WOA. Furthermore, the shortest navigation time corresponds to the maximum rotational angular velocity. Consequently, in the subsequent study on the encounter probability, the rotational angular velocity of the supercavitating vehicle is set as 40°/s.

TABLE 2. Minnimum navigation time of 4 optimization algorithms.

Algorithm	CG-P-PSO	PSO	ABC	WOA
Min navigation time(s)	91.6821	90.7733	91.6925	91.6821
Number of min navigation time	75	1	1	1
Fitness value(m)	1e-6	63.0513	0.9347	0.0013
w(rad/s)	-0.6981	-0.4731	-0.6734	-0.6981
t_t(s)	0.7529	1.1215	0.7809	0.7530
t_s(s)	90.9291	89.6517	90.9116	90.9291

III. JUDGEMENT INDEX OF ENCOUNTER PROBABILITY ANALYTIC MODEL

In order to establish the analytic model of the encounter probability between the supercavitating vehicle and the target, it is essential to determine the judgement indexes of the encounter probability in SRM and TSRM. In previous studies, the coordinates of the intersection point between the supercavitating vehicle path and target path as well as the miss distance are directly used as judgement indexes. However, few papers have thoroughly examined their validity. In this section, the Monte Carlo simulation method is used to determine the judgement indexes of the encounter probability in two modes and verify the probability distribution characteristics. Additionally, the Monte Carlo simulation method for encounter probability considering the target scale is presented.

A. MONTE CARLO SIMULATION METHOD

As shown in Fig. 2, the coordinates of the four vertices of the target contour in $X_BO_BZ_B$ are shown in (9).

$$\begin{cases} A_1 = [-\dfrac{L_m}{2}, -\dfrac{B_m}{2}] \\ A_2 = [-\dfrac{L_m}{2}, \dfrac{B_m}{2}] \\ A_3 = [\dfrac{L_m}{2}, -\dfrac{B_m}{2}] \\ A_4 = [\dfrac{L_m}{2}, \dfrac{B_m}{2}] \end{cases} \tag{9}$$

At any time t, the coordinates of the four vertices of the target contour in $X_EO_EZ_E$ are formulated in (10), and then the analytic expression of the target contour during navigation is derived as (11).

$$A_i^E = R_{BE}A_i^T + [x_m^E, z_m^E]^T, i = 1, 2, 3, 4 \tag{10}$$

$$\begin{cases} x_1 = \dfrac{\cos C_m}{\sin C_m} z_1 + \dfrac{B_m}{2\sin C_m} + \dfrac{D_s \sin(C_m - B_s)}{\sin C_m} \\ x_2 = \dfrac{\cos C_m}{\sin C_m} z_2 - \dfrac{B_m}{2\sin C_m} + \dfrac{D_s \sin(C_m - B_s)}{\sin C_m} \\ x_3 = -\dfrac{\sin C_m}{\cos C_m} z_3 + \dfrac{D_s \cos(C_m - B_s)}{\cos C_m} - \dfrac{L_m}{2\cos C_m} \\ \quad + \dfrac{V_m t}{\cos C_m} \\ x_4 = -\dfrac{\sin C_m}{\cos C_m} z_4 + \dfrac{D_s \cos(C_m - B_s)}{\cos C_m} + \dfrac{L_m}{2\cos C_m} \\ \quad + \dfrac{V_m t}{\cos C_m} \end{cases} \tag{11}$$

where the transformation matrix from $X_B O_B Z_B$ to $X_E O_E Z_E$ is $R_{BE} = \begin{bmatrix} \cos C_m & -\sin C_m \\ \sin C_m & \cos C_m \end{bmatrix}$.

The criterion for determining the encounter between the supercavitating vehicle and the target is based on whether the supercavitating vehicle can intersect the target contour throughout the entire approach process. Firstly, the trajectory of the supercavitating vehicle and four lines of target contour are solved simultaneously. Encounter time in SRM can be directly expressed as.

$$\begin{cases} t_{s1} = \dfrac{B_m + 2D_s \sin(C_m - B_s)}{2V_s \sin(C_m - C_u)} \\ t_{s2} = \dfrac{2D_s \sin(C_m - B_s) - B_m}{2V_s \sin(C_m - C_u)} \\ t_{s3} = \dfrac{2D_s \cos(C_m - B_s) - L_m}{2V_s \cos(C_m - C_u) - 2V_m} \\ t_{s4} = \dfrac{2D_s \cos(C_m - B_s) + L_m}{2V_s \cos(C_m - C_u) - 2V_m} \end{cases} \tag{12}$$

In TSRM, it is necessary to judge whether the supercavitating vehicle meets the target contour during the turning-running course and the straight-running course after turning, respectively. The encounter time $t_{ti}, i = 1, 2, 3, 4$ between the turning-running course of the supercavitating vehicle and the four lines of the target contour is determined by the dichotomy method. The method of solving the encounter time $t_{tsi}, i = 1, 2, 3, 4$ between the straight-running course after turning and four lines of the target contour is the same as that used in SRM. t_{tsi} needs to satisfy $[0, (L_{\max} - wt_t)/V_T]$. If encounter time meets at least one condition in (13), the encounter between the supercavitating vehicle and the target is determined. Γ is represented as t_{si}, t_{ti}, and t_{tsi}, $i = 1, 2, 3, 4$, respectively.

$$\text{s.}t. \begin{cases} x_1(\Gamma) \in [A^E_{1,\Gamma}(1), A^E_{3,\Gamma}(1)],\ z_1(\Gamma) \in [A^E_{1,\Gamma}(2), A^E_{3,\Gamma}(2)] \\ x_2(\Gamma) \in [A^E_{2,\Gamma}(1), A^E_{4,\Gamma}(1)],\ z_2(\Gamma) \in [A^E_{2,\Gamma}(2), A^E_{4,\Gamma}(2)] \\ x_3(\Gamma) \in [A^E_{1,\Gamma}(1), A^E_{2,\Gamma}(1)],\ z_3(\Gamma) \in [A^E_{1,\Gamma}(2), A^E_{2,\Gamma}(2)] \\ x_4(\Gamma) \in [A^E_{3,\Gamma}(1), A^E_{4,\Gamma}(1)],\ z_{4,}(\Gamma) \in [A^E_{3,\Gamma}(2), A^E_{4,\Gamma}(2)] \end{cases} \tag{13}$$

B. MONTE CARLO SIMULATION ANALYSIS

Monte Carlo simulations in SRM and TSRM are conducted to calculate the encounter probability with the relevant parameters outlined in Table 3. Three typical scenarios are constructed by considering different typical azimuth angles. The initial heading C_{ut} in TSRM is obtained by adding the same angle $\alpha = 30^\circ$ to the heading angle C_u in SRM. The path information is obtained by the encounter analytic model proposed in this paper, as shown in Table 4. The mean square error of each parameter is shown in Table 5. Generally, in accordance with the central limit theorem, the random error during the approach process follows a standard normal distribution [34].

The number of Monte Carlo simulations N is set to 5000. N_h denotes the number of simulations satisfying Equation (13). Consequently, the encounter probability can be expressed as $P = N_h/N$. The simulation results show that the encounter probabilities in SRM are 30.52%, 32.32%, and 39.92%, respectively. Meanwhile, the encounter probabilities in TSRM are 16.8%, 22.38%, and 22.28%, respectively. In SRM, the coordinate X_B of the intersection point between the supercavitating vehicle path and target path in $X_B O_B Z_B$ is used as the judgement index of the encounter probability. In TSRM, the miss distance $r_{\min}$ is employed as the judgement index of the encounter probability. $r_{\min}$ demonstrates the shortest distance between the supercavitating vehicle and the target centroid during the entire approach process. Fig. 6-9 illustrate the statistical characteristics of the two judgement indexes. It can be seen from Fig. 6 and Fig. 8 that the distributions and the empirical CDF of the two judgement indexes fit the fitted PDF and theoretical CDF well, respectively. As shown in Fig. 7 and Fig. 9, the

TABLE 3. Monte carlo simulation parameters.

	D_s (m)	C_M (°)	B_s (°)	V_m (kn)	C_{ut} (°)	V_s (kn)
SRM	6000	90	[45,0,315]	30	—	150
TSRM	6000	90	[45,0,315]	30	[83.13,41.54,35 3.13]	150

TABLE 4. Path parameters of supercavitating vehicle.

	Parameters	C_u(°)	W(°/s)	t_t(s)
Scenario 1	SRM	53.1301	—	—
	TSRM	—	-40	0.7529
Scenario 2	SRM	11.5370	—	—
	TSRM	—	-40	0.7534
Scenario3	SRM	323.1301	—	—
	TSRM	—	-40	0.7539

TABLE 5. Standard deviation of random errors.

Standard deviation	σ_{B_s}	σ_{D_s}	σ_{V_m}	σ_{C_m}	$\sigma_{C_{ut}}$	σ_{C_u}	σ_{V_s}	σ_w
Unit	°	m	kn	°	°	°	kn	°/s
Value	0.3	10	5	1.5	0.3	0.3	5	3

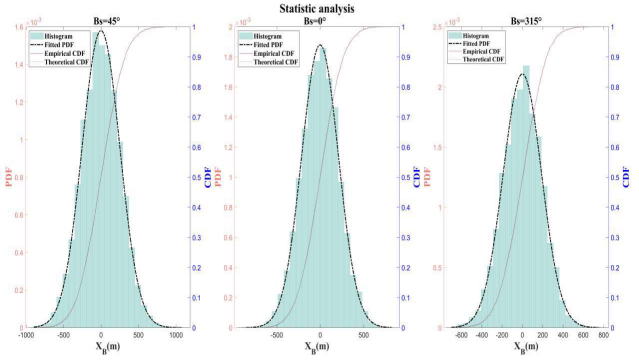

FIGURE 6. Distribution of X_B in three scenarios in SRM.

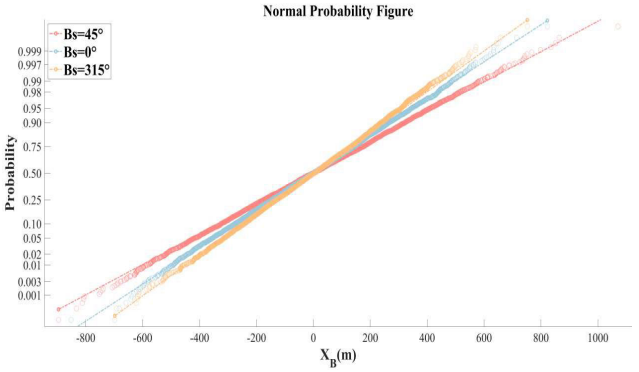

FIGURE 7. Normal probability plot of X_B in three scenarios in SRM.

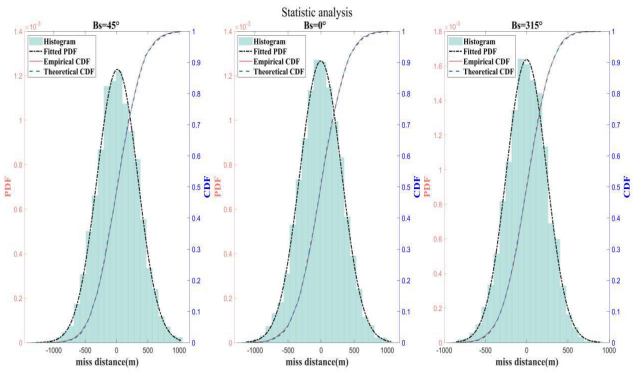

FIGURE 8. Distribution of r_{min} in three scenarios in TSRM.

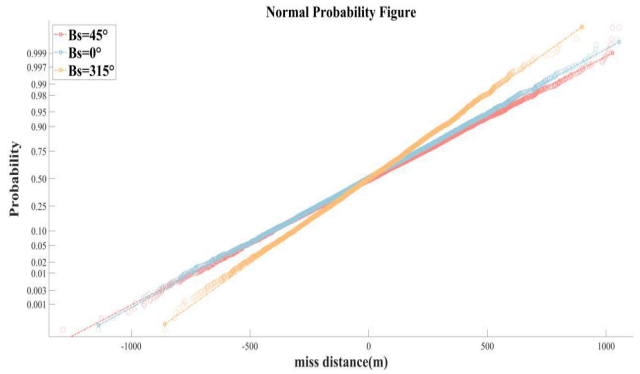

FIGURE 9. Normal probability plot of r_{min} in three scenarios in TSRM.

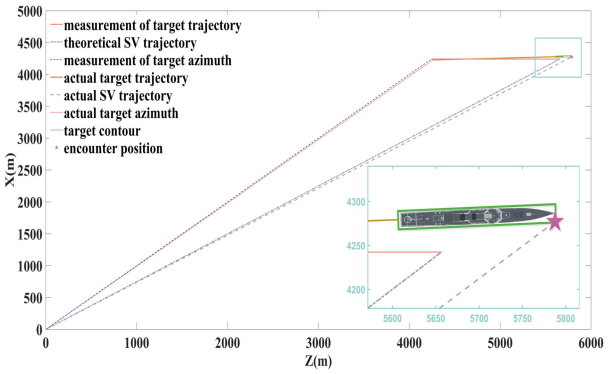

(a) Maximum X_B

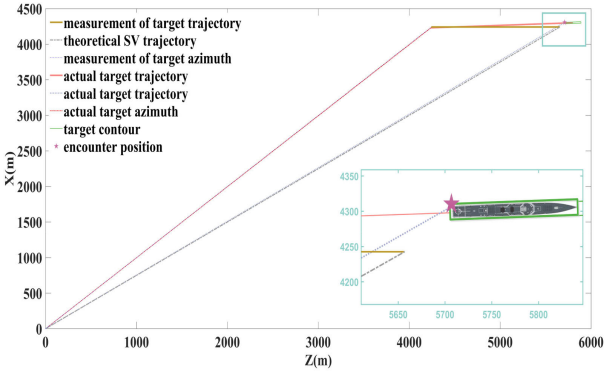

(b) Minimum X_B

FIGURE 10. The encounter situation diagram corresponding to the maximum and minimum X_B in scenario 2.

distributions of the two judgement indexes fit the normal probability well, respectively. In summary, the two judgement indexes basically obey the standard normal distribution. Hypothesis testing will be used for further verification in the subsequent sections. Fig. 10 demonstrates the encounter situation diagrams corresponding to the maximum and minimum judgement index X_B of SRM in scenario 2. It can be observed that the boundary conditions of the encounter are X_B corresponding to the two paths with the largest slope and the smallest slope of the four paths that the supercavitating vehicle encounters the four vertices of the target contour.

IV. ENCOUNTER PROBABILITY ANALYTIC MODEL

In this section, the analytic expressions of X_B in SRM and $r_{\min}$ in TSRM are derived. According to the law of error propagation, the implicit function differential method is adopted to obtain the analytic models of the judgement indexes X_B and $r_{\min}$ considering the random errors comprehensively during the entire approach process. The integral intervals in two modes are determined based on the relative motion between the supercavitating vehicle and the target.

A. STRAIGHT-RUNNING MODE

According to the measurement parameters, the path of the target centroid can be expressed as follows.

$$x_m = \frac{\cos C_m}{\sin C_m} z_e + \frac{D_s \sin(C_m - B_s)}{\sin C_m} \tag{14}$$

Substitute the path of the supercavitating vehicle in SRM into (14) to obtain the time t_{en} expressed as (15) at which the supercavitating vehicle reaches the target path. The geodetic coordinates at t_{en} are obtained and expressed as (16).

$$t_{en} = \frac{D_s \sin(C_m - B_s)}{V_s \sin(C_m - C_u)} \tag{15}$$

$$\begin{cases} x_{sE} = \dfrac{D_s \sin(C_m - B_s)\cos C_u}{\sin(C_m - C_u)} \\ z_{sE} = \dfrac{D_s \sin(C_m - B_s)\sin C_u}{\sin(C_m - C_u)} \end{cases} \tag{16}$$

The coordinate x_{sE} is transformed to obtain X_B from $X_E O_E Z_E$ to $X_B O_B Z_B$ through the transformation matrix R_{EB}.

$$X_B = D_s\left(\frac{\sin(C_u - B_s)}{\sin(C_m - C_u)} - \frac{V_m \sin(C_m - B_s)}{V_s \sin(C_m - C_u)}\right) \tag{17}$$

Equation (17) is rewritten as $X_B = f(D_s, B_s, C_m, V_m, C_u, V_s)$. Based on the law of error propagation, the variance of X_B can be represented as (18). According to (3) and (10), the distances ξ_{tv}^i, $i = 1, 2, 3, 4$ between the supercavitating vehicle and the four vertices of the target contour can be expressed in (19). The initial heading C_{ui} of the supercavitating vehicle and the encounter time t_s are the variables to be determined by the classical PSO. Subsequently, the maximum heading C_{umax} and minimum heading $C_{u\min}$ among C_{ui} are obtained. The integral interval $[X_{B\min}, X_{Bmax}]$ is obtained according to (17).

$$\begin{cases} D_{X_B} = KDK^T \\ K = [\dfrac{\partial f}{\partial D_s}, \dfrac{\partial f}{\partial B_s}, \dfrac{\partial f}{\partial C_m}, \dfrac{\partial f}{\partial V_m}, \dfrac{\partial f}{\partial C_u}, \dfrac{\partial f}{\partial V_s}] \\ D = diag([\sigma_{D_s}^2, \sigma_{B_s}^2, \sigma_{C_m}^2, \sigma_{V_m}^2, \sigma_{C_u}^2, \sigma_{V_s}^2]) \end{cases} \tag{18}$$

$$\begin{cases} \min \xi_{tv}^i = \sqrt{(x_{s\_s}^E - A_i^E(1))^2 + (z_{s\_s}^E - A_i^E(2))^2}, \\ \quad i = 1, 2, 3, 4 \\ s.t. \begin{cases} C_{ui} \in [0, 2\pi] \\ t_i \in (0, L_{\max}/V_s] \end{cases} \end{cases} \tag{19}$$

The analytic model of the encounter probability in SRM can be expressed as $P = \int_{X_{B\min}}^{X_{Bmax}} \frac{1}{\sqrt{2\pi D_{X_B}}} e^{-\frac{X_B^2}{2D_{X_B}}} dx_B$.

B. TURNING-STRAIGHT-RUNNING MODE

Since the TSRM path of the supercavitating vehicle comprises turning-running course and straight-running course, the random error of the angular velocity results in initial position dispersion of the straight-running course. As a result, the analytic model of the encounter probability in TSRM of the supercavitating vehicle is derived by segmentation method.

The position of the supercavitating vehicle after turning can be expressed as (20). C_{ue} denotes the heading of the supercavitating vehicle after turning.

$$\begin{cases} x_{tse} = \dfrac{V_S}{w}\sin(C_{ue}) - \dfrac{V_S}{w}\sin(C_{ut}) \\ z_{tse} = -\dfrac{V_S}{w}\cos(C_{ue}) + \dfrac{V_S}{w}\cos(C_{ut}) \\ C_{ue} = C_{ut} + wt_t \end{cases} \tag{20}$$

According to the law of error propagation, the position variances of the supercavitating vehicle after turning can be derived as.

$$\begin{cases} \sigma x_{tse}^2 = (\dfrac{\partial x_{tse}}{\partial V_S})^2 \sigma V_S^2 + (\dfrac{\partial x_{tse}}{\partial w})^2 \sigma w^2 + (\dfrac{\partial x_{tse}}{\partial C_{ut}})^2 \sigma C_{ut}^2 \\ \sigma z_{tse}^2 = (\dfrac{\partial z_{tse}}{\partial V_S})^2 \sigma V_{Ss}^2 + (\dfrac{\partial z_{tse}}{\partial w})^2 \sigma w^2 + (\dfrac{\partial z_{tse}}{\partial C_{ut}})^2 \sigma C_{ut}^2 \\ \sigma C_{ue}^2 = \sigma C_{ut}^2 + \sigma w^2 t_t^2 \end{cases} \tag{21}$$

After the supercavitating vehicle turns, the geodetic coordinates of the target centroid are expressed as.

$$\begin{cases} x_{me} = D_s \cos B_s + V_m t_t \cos C_m \\ z_{me} = D_s \sin B_s + V_m t_t \sin C_m \end{cases} \tag{22}$$

Accordingly, the target position variances can be determined as.

$$\begin{cases} \sigma x_{me}^2 = (\dfrac{\partial x_{me}}{\partial D_s})^2 \sigma D_s^2 + (\dfrac{\partial x_{me}}{\partial B_s})^2 \sigma B_s^2 + (\dfrac{\partial x_{me}}{\partial V_m})^2 \sigma V_m^2 \\ +(\dfrac{\partial x_{me}}{\partial C_m})^2 \sigma C_m^2 \\ \sigma z_{me}^2 = (\dfrac{\partial z_{me}}{\partial D_s})^2 \sigma D_s^2 + (\dfrac{\partial z_{me}}{\partial B_s})^2 \sigma B_s^2 + (\dfrac{\partial z_{me}}{\partial V_m})^2 \sigma V_m^2 \\ +(\dfrac{\partial z_{me}}{\partial C_m})^2 \sigma C_m^2 \end{cases} \tag{23}$$

The Monte Carlo method is employed to simulate position dispersion of the supercavitating vehicle and the target after turning-running time in Scenario 1, as shown in Fig. 11-13. From the simulation results, it is evident that the positions of the target and the supercavitating vehicle after turning-running time follow a normal distribution with the mean values calculated based on the measurement parameters.

During the straight-running course of the supercavitating vehicle, the relative motion of the supercavitating vehicle with the target can be derived as follows.

$$\begin{cases} \dot{r} = V_m \cos(C_m - q) - V_S \cos(C_{ue} - q) \\ r\dot{q} = V_m \sin(C_m - q) - V_S \sin(C_{ue} - q) \end{cases} \tag{24}$$

where r denotes the distance between the supercavitating vehicle and the target centroid. q denotes the time-variant line of sight angle.

Divide the first formula by the second formula in (24), and integrate simultaneously yields as follows.

$$\ln r = \int \frac{d(V_S \sin(C_{ue} - q) - V_m \sin(C_m - q))}{V_S \sin(C_{ue} - q) - V_m \sin(C_m - q)} \tag{25}$$

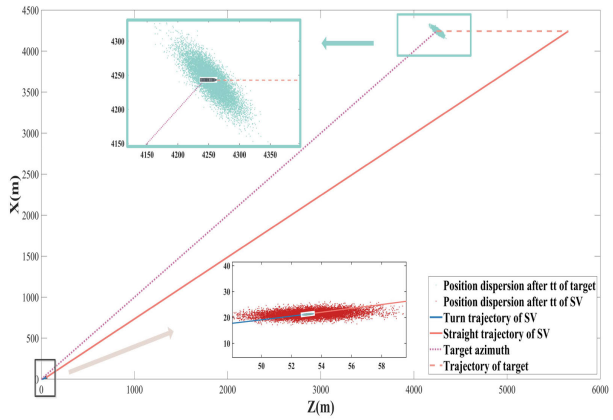

FIGURE 11. The position dispersion diagram of the supercavitating vehicle and the target.

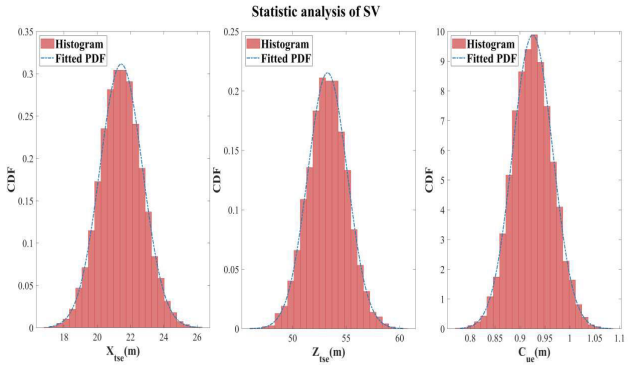

FIGURE 12. The statistical analysis of position dispersion of the supercavitating vehicle.

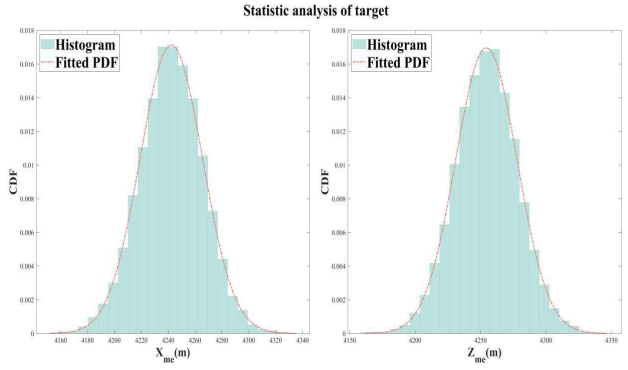

FIGURE 13. The statistical analysis of position dispersion of the target.

The distance D_{Se} and azimuth angle B_{Se} between the supercavitating vehicle and the target after the turning-running time are regarded as the initial values in (25). The mathematical expression of r is given as follows.

$$r = \frac{D_{se}[V_m \sin(C_m - B_{se}) - V_S \sin(C_{ue} - B_{se})]}{V_m \sin(C_m - q) - V_S \sin(C_{ue} - q)} \tag{26}$$

$$D_{Se} = \sqrt{(\Delta x)^2 + (\Delta z)^2} \tag{27}$$

$$B_{Se} = \begin{cases} \arccos \dfrac{\Delta x}{\sqrt{\Delta x^2 + \Delta z^2}}, & \Delta z > 0 \\ 2\pi - \arccos \dfrac{\Delta x}{\sqrt{\Delta x^2 + \Delta z^2}}, & \Delta z < 0 \\ 0, & \Delta z = 0, \Delta x > 0 \\ \pi, & \Delta z = 0, \Delta x < 0 \end{cases} \tag{28}$$

where $\Delta x = x_{tse} - x_{me}$ and $\Delta z = z_{tse} - z_{me}$.

Equation (29) is obtained by simplifying (26). ΔV_x and ΔV_z denote the projections of the relative velocity between the supercavitating vehicle and the target in $X_E O Z_E$.

$$\begin{cases} r = \dfrac{D_{Se} \sin(\beta - B_{Se})}{\sin(\beta - q)} \\ \tan\beta = \dfrac{\Delta V_z}{\Delta V_x} \\ \Delta V_x = V_m \cos C_m - V_S \cos C_{ue} \\ \Delta V_z = V_m \sin C_m - V_S \sin C_{ue} \end{cases} \tag{29}$$

where D_{se}, β and B_{se} can be described as $\begin{cases} D_{se} = \kappa(x_{me}, z_{me}, x_{tse}, z_{tse}) \\ \zeta(\beta, C_m, C_{ue}, V_s, V_m) = 0 \\ \psi(B_{se}, x_{me}, z_{me}, x_{tse}, z_{tse}) = 0 \end{cases}$, the corresponding variances can be expressed as.

$$\begin{cases} \sigma D_{Se}^2 = (\dfrac{\partial D_{Se}}{\partial x_{me}})^2 \sigma x_{me}^2 + (\dfrac{\partial D_{Se}}{\partial x_{tse}})^2 \sigma x_{tse}^2 + (\dfrac{\partial D_{Se}}{\partial z_{tse}})^2 \sigma z_{tse}^2 \\ +(\dfrac{\partial D_{Se}}{\partial z_{me}})^2 \sigma z_{me}^2 \\ \sigma\beta^2 = (\dfrac{\partial \beta}{\partial C_m})^2 \sigma C_m^2 + (\dfrac{\partial \beta}{\partial C_{ue}})^2 \sigma C_{ue}^2 + (\dfrac{\partial \beta}{\partial V_S}) \sigma V_S^2 \\ +(\dfrac{\partial \beta}{\partial V_m})^2 \sigma V_m^2 \\ \sigma B_{Se}^2 = (\dfrac{\partial B_{Se}}{\partial x_{tse}})^2 \sigma x_{tse}^2 + (\dfrac{\partial B_{Se}}{\partial x_{me}})^2 \sigma x_{me}^2 + (\dfrac{\partial B_{Se}}{\partial z_{me}})^2 \sigma z_{me}^2 \\ +(\dfrac{\partial B_{Se}}{\partial z_{tse}})^2 \sigma z_{tse}^2 \end{cases} \tag{30}$$

When $\dot{r} = 0$, the distance between the supercavitating vehicle and the target centroid is shortest, that is, the miss distance $r_{\min}$.The miss distance can be expressed as $r_{\min} = D_{se} \sin(\beta - B_{se})$. Similarity, the variance of the miss distance can be derived as $\sigma r_{\min}^2 = (\frac{\partial r}{\partial D_{Se}})^2 \sigma D_{Se}^2 + (\frac{\partial r}{\partial \beta})^2 \sigma\beta^2 + (\frac{\partial r}{\partial B_{Se}})^2 \sigma B_{Se}^2$ following a standard normal distribution $\mathcal{N}(0, \sigma r_{\min})$. The method for determining the integral interval of the encounter probability analytic model in TSRM is similar to that in SRM. Initially, the classical PSO is adopted to obtain the four paths that the supercavitating vehicle encounters the four vertices of the target contour as it moves from the initial position of the straight-running course, which correspond to four heading angles C_{ue_bi}, $i = 1, 2, 3, 4$. Combining (27)-(29), the four miss distances corresponding to the four heading angles can be obtained, in which the maximum and minimum miss distances are the integral interval.

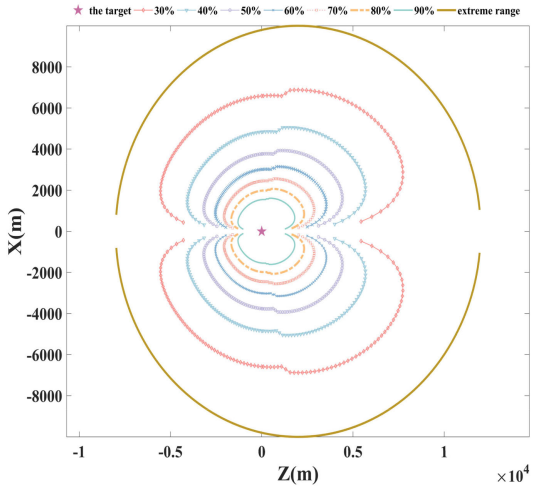

FIGURE 14. Equal encounter probability positions and extreme range of the supercavitating vehicle.

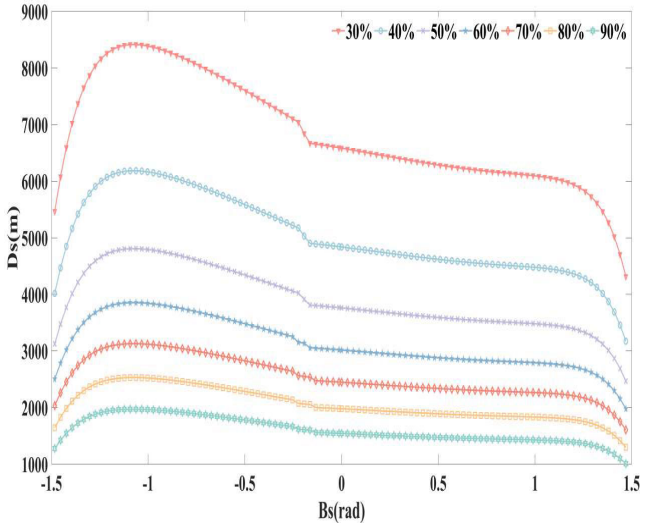

FIGURE 15. Change curves of ranges with azimuth angles.

V. SIMULATION VERIFICATION

Based on the encounter probability analytic models in SRM and TSRM, the encounter probabilities in two modes under different scenarios are calculated. The accuracy of the proposed analytic methods is validated through comparison with the Monte Carlo simulation results. The number of Monte Carlo simulations is set to 5000.

A. STRAIGHT-RUNNING MODE

The extreme range of the supercavitating vehicle and the positions with equal encounter probability are crucial for strike decision-making. The extreme range $D_{s\max}$ under different scenarios is computed according to (31). Azimuth angles are designated to $[0, 85°] \cup [275°, 360°]$, with an interval of 0.03rad. In the case of conventional torpedoes, the positions with the equal hit probability commonly involve three hit probabilities of 0.9, 0.8 and 0.5 [46]. In this paper, the equal encounter probabilities are set from 0.3 to 0.9, with an interval of 0.1. The classical PSO is employed to calculate the range D_s corresponding to the anticipated encounter probability P_d according to the objective function (32).

$$D_{s\max} = \frac{L_{\max}\sin(Q_m + \varphi)}{\sin(Q_m)} \tag{31}$$

$$\begin{cases} \min \mathrm{J} = |P - P_d| \\ s.t. 0 < D_s < D_{s\max} \end{cases} \tag{32}$$

As depicted in Fig. 14, the positions with the equal encounter probability of the supercavitating vehicle do not form a regular circle, and the trend of the positions of each equal encounter probability remains consistent. Fig. 15 illustrates the relationship between the range and the azimuth angle. The trend reveals that the range initially increases and subsequently decreases as the azimuth angle increases. In other words, achieving the desired encounter probability requires a shorter range for either excessively large or small bearing angles. Table 6 presents the parameters associated with the maximum range of each equal encounter probability. According to the encounter time corresponding to the maximum range of different encounter probabilities, it is apparent that the maximum encounter time does not exceed 2 minutes, which highlights the rapidity of the supercavitating vehicle. Consequently, the target has insufficient time to maneuver or implement countermeasures.

TABLE 6. Relative parameters of maximum ranges.

Encounter probability	$D_{s\max}$ (m)	B_s (°)	Q_m (°)	Incidence angle (°)	Encounter time (s)
30%	8415.775	-60.936	29.064	34.6398	109.069
40%	6183.791	-60.936	29.064	34.6398	80.142
50%	4807.780	-60.936	29.064	34.6398	62.309
60%	3853.054	-60.936	29.064	34.6398	49.936
70%	3128.824	-60.936	29.064	34.6398	40.550
80%	2530.363	-60.936	29.064	34.6398	32.794
90%	1971.378	-60.936	29.064	34.6398	25.549

TABLE 7. Deviation between analytic method and monte carlo simulation.

Deviation	Number	Proportion
[0,0.01]	575	82.14%
(0.01,0.02]	109	15.57%
(0.02,0.03]	9	1.29%
(0.03,0.04]	6	0.86%
(0.04,0.05]	1	0.14%

The Monte Carlo simulation method is used to calculate the encounter probabilities for 700 positions of 7 equal encounter probabilities. The encounter probability deviations of the two methods are summarized in Table 7. Fig.16 illustrates the

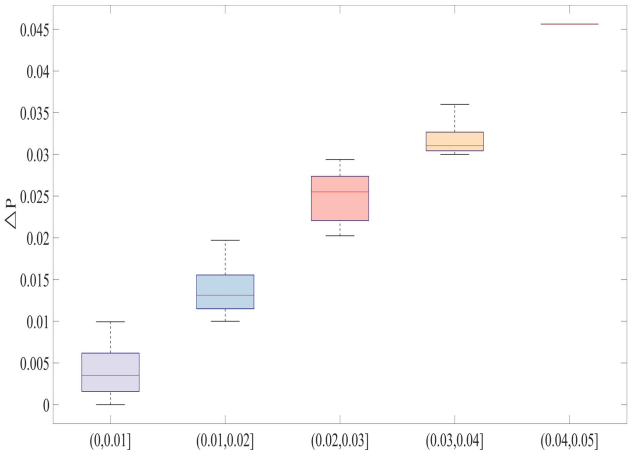

FIGURE 16. Box diagram of encounter probability deviation.

TABLE 8. Deviation between analytic method and monte carlo simulation.

Deviation	Number	Proportion
[0,0.01]	79	34.2%
(0.01,0.02]	67	29%
(0.02,0.03]	32	13.85%
(0.03,0.04]	22	9.52%
(0.04,0.05]	16	6.93%
(0.06,0.07]	6	2.6%
(0.07,0.08]	8	3.46%
(0.08,0.09]	1	0.43%

distribution of encounter probability deviations between the two methods across different ranges, and the results can verify the precision of the encounter probability analytic model in SRM proposed in this paper.

B. TURNING-STRAIGHT-RUNNING MODE

The ranges of the supercavitating vehicle in TSRM are set from 1000m to 7000m, with an interval of 1000m. The azimuth angle range is set to $[0, 80°] \cup [280°, 355°]$, with an interval of 5°. The encounter probabilities obtained from the analytic method and Monte Carlo simulation are shown in Fig. 17, while the deviations of two methods are listed in Table 8. According to the results, the deviation accuracy between the analytic method and Monte Carlo simulation in TSRM is slightly lower than that in SRM, but the number of deviations greater than 5% accounts for only 6.49%, affirming the feasibility and effectiveness of the encounter probability analytic model in TSRM. Fig. 17 indicates a consistent trend in the encounter probabilities across different ranges and azimuth angles. The larger deviation may be attributed to the introduction of turning angular velocity error of the supercavitating vehicle, rendering the Monte Carlo simulation more complex and increasing result uncertainty.

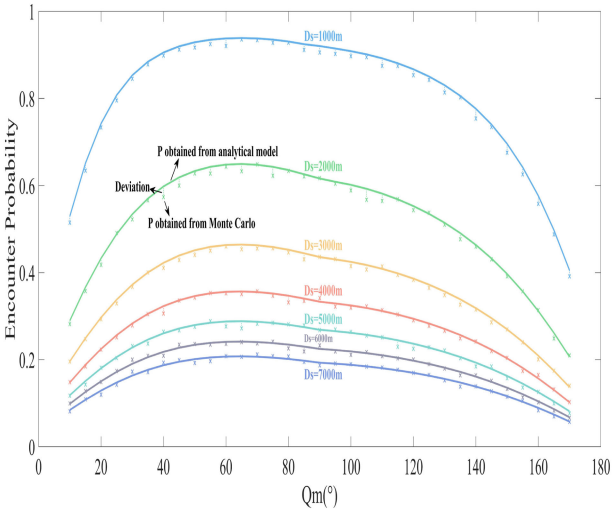

FIGURE 17. Encounter probabilities in TSRM.

TABLE 9. Results of the hypothesis testing.

	Scenario	$\sigma_{D_{Se}}$	confidence interval	$\bar{D}_{Se}$	hypothesis
SRS	1	252.60	[-7.79 ,6.21]	-0.7880	H_0
	2	212.86	[-8.22,3.58]	-2.3213	H_0
	3	191.72	[-5.52,5.11]	-0.2072	H_0
TSRS	1	325.72	[5.80,23.86]	14.8308	H_0
	2	315.47	[-13.60,3.89]	-4.8583	H_0
	3	244.04	[-7.77,5.75]	-1.0096	H_0

C. HYPOTHESIS TESTING

In reference to Section III, the judgement indexes of the encounter probability in both SRM and TSRM are statistically analyzed, respectively. This analysis then forms the basis for deriving the analytic models of two judgement index variance. However, the rationality whether the judgement indexes conform to the standard normal distribution needs further verification. In this section, hypothesis testing based on unbiased estimation is used to verify the rationality of the assumption that the means of the judgement indexes X_B and $r_{\min}$ are zero.

The original hypothesis H_0 is denoted as $\mu = \mu_0(0)$. The alternative hypothesis H_1 is denoted as $\mu \neq \mu_0$. Based on (33), the range of μ satisfying the confidence level is $[\mu_0 - u_{\alpha/2}\sigma_0 \big/ \sqrt{N}, \mu_0 + u_{\alpha/2}\sigma_0 \big/ \sqrt{N}]$. Here, $u_{\alpha/2}$ signifies the quantile $\alpha/2$ of the standard normal distribution. The significance level α is set to 0.05. The results are listed in Table 9. In accordance with the principle of small probability, the original hypotheses are accepted for both SRM and TSRM under three typical scenarios. Therefore, it is further verified that the judgement indexes of the encounter probability analytic models in SRM and TSRM obey the standard normal distributions.

$$P\left\{\left|\bar{X} - \mu_0\right| \geq k\right\} = \alpha \tag{33}$$

where $\bar{X}$ represents the sample mean of the judgement indexes X_B and $r_{\min}$.

VI. CONCLUSION

This paper conducts research on the encounter probability between the supercavitating vehicle in SRM and TSRM with the target. In SRM, the mathematical encounter model is established, utilizing the advanced angle mode. For TSRM path planning, an improved PSO (named CG-P-PSO) based on the local best topology is proposed. The particle position update employs Cauchy and Gaussian distributions, and a penalty function is integrated to drive the optimization algorithm to obtain the optimal path with the shortest encounter time. The superior robustness and accuracy of CG-P-PSO are validated through comparison with other optimization algorithms. The Monte Carlo method considering the target scale is employed to determine the judgement indexes of the encounter probability analytic model in SRM and TSRM. Statistical analysis confirms that these indexes adhere to the standard normal distribution. Furthermore, based on the law of error propagation, the analytic models of the two judgement index variances are derived using the implicit function differential method. The strategy for determining the integral intervals is proposed based on the relative motion between the supercavitating vehicle and the target. Finally, the accuracy and feasibility of the encounter probability analytic model in SRM and TSRM are validated through Monte Carlo simulation and the hypothesis testing method. Future work will include multi-target optimization research to maximize the encounter probability [47] and the study of the trajectory dispersion.

REFERENCES

[1] K. Ng, "Overview of the ONR supercavitating high-speed bodies program," in *Proc. AIAA Guid., Navigat., Control Conf. Exhib.*, Aug. 2006, pp. 21–24.

[2] X. Yuan and T. Xing, "Hydrodynamic characteristics of a supercavitating vehicle's aft body," *Ocean Eng.*, vol. 114, pp. 37–46, Mar. 2016, doi: 10.1016/j.oceaneng.2016.01.012.

[3] K. Zhang, P. Li, Z. Wang, K. Yan, and W. Chen, "Experimental study of planning force on supercavitating vehicle tail," *J. Ship Mech.*, vol. 24, no. 1, pp. 8–17, Jan. 2020, doi: CNKI:SUN:CBLX.0.2020-01-002.

[4] H. Mokhtarzadeh, G. Balas, and R. Arndt, "Effect of cavitator on supercavitating vehicle dynamics," *IEEE J. Ocean. Eng.*, vol. 37, no. 2, pp. 156–165, Apr. 2012.

[5] R. Lu, G. Pan, K. Tan, and S. Yin, "Numerical simulation of cavitation and damping force characteristics for a high-speed supercavitation vehicle," *J. Mar. Sci. Eng.*, vol. 9, no. 11, p. 1171, Oct. 2021, doi: 10.3390/jmse9111171.

[6] M. Wang, C. Fan, and G. Hou, "Numerical research of lateral flow influence on supercavitating flow," *AIP Adv.*, vol. 12, no. 4, Apr. 2022, Art. no. 045214.

[7] B.-K. Ahn, T.-K. Lee, H.-T. Kim, and C.-S. Lee, "Experimental investigation of supercavitating flows," *Int. J. Nav. Archit. Ocean Eng.*, vol. 4, no. 2, pp. 123–131, Jun. 2012.

[8] J. Dzielski and A. Kurdila, "A benchmark control problem for supercavitating vehicles and an initial investigation of solutions," *J. Vibrat. Control*, vol. 9, no. 7, pp. 791–804, Jul. 2003.

[9] S. Kim and N. Kim, "Control method for ventilated supercavitating vehicle considering planing avoidance and stability," *Proc. Inst. Mech. Eng., M, J. Eng. Maritime Environ.*, vol. 233, no. 3, pp. 957–968, Aug. 2019, doi: 10.1177/1475090218798404.

[10] X. Mao and Q. Wang, "Delay-dependent control design for a time-delay supercavitating vehicle model," *J. Vibrat. Control*, vol. 17, no. 3, pp. 431–448, Mar. 2011.

[11] X. Zhao, X. Zhang, X. Ye, and Y. Liu, "Sliding mode controller design for supercavitating vehicles," *Ocean Eng.*, vol. 184, pp. 173–183, Jul. 2019.

[12] W. Jinghua, L. Yang, C. Guohua, Z. Yongyong, and Z. Jiafeng, "Design of RBF adaptive sliding mode controller for a supercavitating vehicle," *IEEE Access*, vol. 9, pp. 39873–39883, 2021, doi: 10.1109/ACCESS.2021.3063192.

[13] Y. Han, Z. Xu, and H. Guo, "Robust predictive control of a supercavitating vehicle based on time-delay characteristics and parameter uncertainty," *Ocean Eng.*, vol. 237, Oct. 2021, Art. no. 109627.

[14] F.-Z. Zhang, G.-J. Li, J.-H. Wang, and F.-Q. Ma, "Characteristics simulation of supercavitation vehicle bubble noise," *Tech. Acoust.*, vol. 35, no. 3, pp. 127–132, Jun. 2016.

[15] R. Wang, C. Liu, S. Zhao, and X. Qi, "Numerical simulation for rotating motion of a natural super-cavitating vehicle," *J. Vib. Shock*, vol. 39, no. 21, pp. 65–70, Apr. 2020, doi: 10.13465/j.cnki.jvs.2020.21.009.

[16] X.-H. Zhao, Y. Sun, G.-L. Zhao, and J.-L. Fan, "μ-synthesis robust controller design for the supercavitating vehicle based on the BTT strategy," *Ocean Eng.*, vol. 88, pp. 280–288, Sep. 2014.

[17] Y. N. Savchenko, V. N. Semenenko, and G. Y. Savchenko, "Peculiarities of supercavitating vehicles' maneuvering," *Int. J. Fluid Mech. Res.*, vol. 46, no. 4, pp. 309–323, 2019, doi: 10.1615/InterJFluidMechRes.v46.i4.30.

[18] G. Yang, F. Lu, and J. Xu, "Research on lateral maneuverability of a supercavitating vehicle based on RBFNN adaptive sliding mode control with rolling restriction and planing force avoidance," *Machines*, vol. 11, no. 8, p. 845, Aug. 2023.

[19] B. Li and T. Liang, "Generalization and application of shooting models of submarine-launched torpedo," *TORPEDO Technol.*, vol. 21, no. 5, pp. 384–387, Oct. 2013.

[20] J. Wu, J. Mao, and W. Ding, "Modeling of submarine torpedo-launching simulation," *J. Syst. Simul.*, vol. 30, no. 3, pp. 873–879, Mar. 2018.

[21] Y. Gong, Z. Wu, and Z. Liu, "Optimal modeling of two-time rotating angle shoot target for accoustic homing torpedo," *Fire Control Command Control*, vol. 43, no. 7, pp. 82–85, Jul. 2018.

[22] Y. Meyer, P. Isaiah, and T. Shima, "On Dubins paths to intercept a moving target," *Automatica*, vol. 53, pp. 256–263, Mar. 2015.

[23] R. Szczepanski, T. Tarczewski, and K. Erwinski, "Energy efficient local path planning algorithm based on predictive artificial potential field," *IEEE Access*, vol. 10, pp. 39729–39742, 2022.

[24] N. Wang, T. Wang, Z. Zhang, S. Shao, Y. Jiang, and Y. Li, "Mobile robot path planning method based on an improved A* algorithm," in *Proc. 12th Int. Conf. CYBER Technol. Autom., Control, Intell. Syst. (CYBER)*, Jul. 2022, pp. 140–143.

[25] V. Roberge, M. Tarbouchi, and G. Labonte, "Comparison of parallel genetic algorithm and particle swarm optimization for real-time UAV path planning," *IEEE Trans. Ind. Informat.*, vol. 9, no. 1, pp. 132–141, Feb. 2013.

[26] Y. Zhang and D. Pang, "Research on path planning of mobile robot based on improved ant colony algorithm," in *Proc. IEEE 6th Inf. Technol. Mechatronics Eng. Conf. (ITOEC)*, vol. 6, Mar. 2022, pp. 558–563.

[27] P. Chen, J. Pei, W. Lu, and M. Li, "A deep reinforcement learning based method for real-time path planning and dynamic obstacle avoidance," *Neurocomputing*, vol. 497, pp. 64–75, Aug. 2022.

[28] W. Jun, L. Yushan, and G. Zhi, "Research on statistic characteristics of the unbiased estimation of hitting probability with rectangle objective domain," in *Proc. 25th Chin. Control Decis. Conf. (CCDC)*, Guiyang, China, May 2013, pp. 2323–2327.

[29] K.-M. Seo, H. S. Song, S. J. Kwon, and T. G. Kim, "Measurement of effectiveness for an anti-torpedo combat system using a discrete event systems specification-based underwater warfare simulator," *J. Defense Model. Simul., Appl., Methodol., Technol.*, vol. 8, no. 3, pp. 157–171, Jul. 2011.

[30] D. Xiaoheng, Z. Yiqi, L. Minghang, and W. Zhengyu, "The surface ship torpedo defense simulation system," in *Proc. IEEE 3rd Int. Conf. Image, Vis. Comput. (ICIVC)*, Jun. 2018, pp. 802–806.

[31] J. Guo, J. Han, X. Li, and Z. Lv, "Search probability analysis of air-dropped torpedo based on Monte Carlo method," *Ordnance Ind. Autom.*, vol. 41, no. 6, pp. 58–62, Apr. 2022.

[32] Z. Cui and Z. Li, "Calculation of detection probability for sub-launch torpedo based on monte-carlo method," *TORPEDO Technol.*, vol. 22, no. 4, pp. 302–305, Aug. 2014.

[33] J. Wang, "Simulation calculation of penetration probability of high speed torpedo attacking surface ship," *Command Control Simul.*, vol. 43, no. 5, pp. 46–50, Oct. 2021.
[34] B.-Q. Wu, X.-C. Guan, S.-H. Guan, and J.-B. Shi, "A capture probability analytic model for the electromagnetic launched anti-torpedo torpedo," *Defence Technol.*, vol. 18, no. 2, pp. 261–270, Feb. 2022.
[35] H. Sun, C. Li, and H. Li, "Hit probability model and simulation of straight-running torpedo," *Ship Electron. Eng.*, vol. 12, no. 12, pp. 138–141, Aug. 2009.
[36] Z. Wu, B. Li, and P. Xia, "An analytic computational method of hitting result for submarine-launched torpedo," *Mathmematics Pract. Theory*, vol. 46, no. 17, pp. 149–153, Sep. 2016, doi: CNKI:SUN:SSJS.0.2016-17-019.
[37] M. Li and Z. Dai, "Analytic method for calculating probability of direct torpedo," *Command Control Simul.*, vol. 39, no. 4, pp. 55–59, Aug. 2017, doi: 10.3969/j.issn.1673-3819.2017.04.012.
[38] C. Xie, J. Zhou, Y. Wan, S. Song, and M. Wang, "Analytical method for hitting probability of supercavitating torpedo salvo," *J. Unmanned Undersea Syst.*, vol. 31, no. 3, pp. 463–473, Dec. 2023.
[39] H. H. Ku, "Notes on the use of propagation of error formulas," *J. Res. Nat. Bur. Standards, Sect. C, Eng. Instrum.*, vol. 70C, no. 4, p. 263, Oct. 1966.
[40] G. Yang, F. Lu, L. Wu, and J. Xu, "Design of particle swarm optimization adaptive sliding mode controller based on an extended state observer for the longitudinal motion of a supercavitating vehicle with input saturation," *J. Sensors*, vol. 2023, pp. 1–23, Feb. 2023.
[41] Y. Zhou, M. Sun, J. Zhang, and Z. Chen, "Depth and attitude coordinated control for supercavitating vehicle avoiding planing force," *Machines*, vol. 10, no. 6, p. 433, Jun. 2022.
[42] X. Li and X. Yao, "Cooperatively coevolving particle swarms for large scale optimization," *IEEE Trans. Evol. Comput.*, vol. 16, no. 2, pp. 210–224, Apr. 2012.
[43] R. C. Eberhart and J. Kennedy, "A new optimizer using particle swarm theory," in *Proc. 6th Int. Symp. Micro Mach. Hum. Sci.*, vol. 1. New York, NY, USA, 1995, pp. 39–43.
[44] S. Ghosh, D. Kundu, K. Suresh, S. Das, A. Abraham, B. K. Panigrahi, and V. Snasel, "On some properties of the lbest topology in particle swarm optimization," in *Proc. 9th Int. Conf. Hybrid Intell. Syst.*, 2009, pp. 370–375.
[45] Y. Zhang, Y. Li, Z. Zhang, F. Luo, and C. Wang, "Multi objective optimization of an asymmetric transmission spindle based on improved particle swarm optimization," *J. Vib. Shock*, vol. 41, no. 2, pp. 130–139, Oct. 2022.
[46] G. Bu and Y. Zhang, "An analytic method to solve the problem of capturing position in launching torpedo," *Ship Sci. Technol.*, pp. 27–32, Mar. 2000, doi: CNKI:SUN:JCKX.0.2000-03-005.
[47] M.-C. Yuen, S.-C. Ng, and M.-F. Leung, "A competitive mechanism multi-objective particle swarm optimization algorithm and its application to signalized traffic problem," *Cybern. Syst.*, vol. 52, no. 1, pp. 73–104, Oct. 2020.

YANG GUANG was born in 1990. He received the B.S. degree in marine and offshore engineering from Harbin Engineering University, in 2013, and the M.S. degree in shipbuilding from the Naval University of Engineering, in 2015, where he is currently pursuing the Ph.D. degree in weapon science and technology. His current research interests include advanced weapon control and multi-agent cooperative control.

LU FAXING was born in 1974. He received the B.S. degree in mine and anti-mine and the M.S. degree in systems engineering from the Naval University of Engineering, in 1997 and 2000, respectively, and the Ph.D. degree in weapon and military technology, military applications and systems from Kuznetsov Naval Academy, Russia, in 2008. He is currently a Professor with the Naval University of Engineering. His current research interests include advanced weapon control and multi-agent cooperative control.

XU JUNFEI was born in 1990. He received the B.S. degree in fire command and control engineering and the joint M.S. and Ph.D. degrees in systems engineering from the Naval University of Engineering, in 2013 and 2019, respectively. He is currently a Lecturer with the Naval University of Engineering. His current research interest includes the assessment of operational effectiveness of naval weapons.

WU LING was born in 1976. She received the B.S. degree from Information Engineering University, the M.S. degree from the Naval University of Engineering, and the Ph.D. degree from Tsinghua University. She is currently a Professor with the Naval University of Engineering. Her research interest includes the field of decision-making for naval combat command assistance.

LI YIYUAN was born in 1997. He received the B.S. and M.S. degrees in radar engineering from the Air Force Early Warning Academy, in 2019 and 2022, respectively. He is currently pursuing the Ph.D. degree in weapon science and technology with the Naval University of Engineering. His current research interests include multi-UAV planning and task allocation.